A Novel Triad Twisted String Actuator for Controlling a Two Degrees of Freedom Joint: Design and Experimental Validation

Damian Crosby[1], Joaquin Carrasco[2], William Heath[2], and Andrew Weightman[1]

Abstract— **Actuated universal joints, or equivalent joint systems, are found in a number of robotic applications, in particular mobile snake robots, continuum robots and robotic tails. These joints have two degrees of freedom on two axes, each perpendicular to a third axis and to themselves. Such joints use a variety of actuation methods, including direct drive motors, linear screw drives, cable based systems, and hydraulics/pneumatics. In this paper the authors design and validate a mechanism that uses the Twisted String Actuator (TSA) in an antagonistic triad to actuate the universal joint, using orientation sensors and load cells to create a robust cascading closed loop control system. This results in a light, compact, high-performance actuation system that avoids the extra mass and hardware complexity that alternative actuation methods present, with the additional challenge of nonlinearity.**

I. INTRODUCTION

Actuated Universal Joint (AUJ) mechanisms are found in a wide range of robotic applications, such as confined space inspection using continuum robots [1], highly manoeuvrable mobile snake robots [2], and biomimetic robot tails for stability [3]. Mobile snake robots must usually incorporate electric actuators inline with their joints. This results in an AUJ having to shift the mass of the follower segments and all the actuators inside the follower segments, which results in high torque requirements. Continuum robots and robotic tails can reduce the mass and size of the AUJ by moving their actuators away from the AUJs and use cables to transfer the force to the joints, or use hydraulic or pneumatic actuators which tend to be lighter than equivalent electric motors. This comes at the expense of increased mass and bulk at the base of the arm or tail.

First developed by Würtz *et al.* [4] in 2010, the Twisted String Actuator (TSA) uses two or more strings between two fixtures as a linear actuator. When one fixture is rotated (typically by an electric motor), the looped string twists into a helix, decreasing the distance between them. TSA actuators have been used for a hand orthosis [5], elbow joint [6] and foldable robot arm [7] among other functions.

The primary advantage of TSA over similar linear actuators such as a leadscrew is the reduction (lower velocity, higher torque) the TSA provides is not proportional to the mass of the actuator, in fact it is slightly inversely proportional. Generally, to increase the reduction in an actuator requires the addition of a gearbox which increases mass, but in the case of the TSA, by decreasing the string cross-section radius, the reduction increases given a constant unwound length and motor angle, resulting in a greater reduction with no increase, or even a slight decrease, in actuator mass.

While the reduction in a leadscrew can be increased by decreasing the lead on the thread, which also has no increase in mass, this has a limited range and can quickly run up against manufacturing tolerances or material strength requirements. In order to achieve greater or more robust reductions, the screw radius has to be increased, or the driving motor has to have a larger reduction before driving the screw, both of which usually result in more material (typically steel) and therefore more mass.

However, TSA does have some disadvantages, the most significant of which is a nonlinear reduction equation, which is also dependent on the motor angle (and therefore actuator position). The reduction decreases in a nonlinear fashion as the angle increases, with the derivative decreasing as the angle increases. There is also the compliance of the strings to consider, depending on the thickness and material chosen, which becomes a significant factor under high forces. Both of these issues can be addressed with accurate modelling [8] and/or a robust control strategy, as demonstrated in [4]. What is more of an issue is the unidirectional force of the TSA, which can only impart force in tension. This means that for an AUJ, which is a 2 Degree of Freedom (DOF) joint, a minimum of three TSA are required, unless spring return mechanisms are used, which would impart additional force on the TSA and therefore reduce performance. However, the potential high force to mass ratio of the TSA due to the non-proportional reduction may adequately compensate for the additional actuator requirement.

The focus of this research is to investigate if the TSA is a suitable candidate for control of an AUJ considering both the benefits and drawbacks. To this end, the objective is to simulate a model and then construct a physical experimental prototype to validate the proposed control system.

TABLE I: Model coefficients.

Coefficient	Value	Coefficient	Value
l_1	$41.8\,\text{mm}$	J	$1 \times 10^{-6}\,\text{kg}\,\text{m}^{-2}$
l_2	$0\,\text{mm}$	K_L	$1000\,\text{N}\,\text{m}^{-1}$
r	$13\,\text{mm}$	$f_{\min}$	$3\,\text{N}$
l_u	$41.8\,\text{mm}$	ω_s	$441.9\,\text{rad}\,\text{s}^{-1}$
r_s	$200\,\mu\text{m}$	I_s	$0.19\,\text{A}$
m	$72.619\,13\,\text{g}$	K_t	$0.0263\,\text{N}\,\text{m}\,\text{A}^{-1}$
C	$0.1315\,\text{N}\,\text{mm}$	τ_s	$4.5\,\text{mN}\,\text{m}$
α_s	$1 \times 10^5\,\text{rad}\,\text{s}^{-2}$		

Coefficient	Value
I	$\begin{bmatrix} 3 \times 10^{-5} & 0 & 0 \\ 0 & 3.2 \times 10^{-5} & 0 \\ 0 & 0 & 1.4 \times 10^{-5} \end{bmatrix}\,\text{kg}\,\text{m}^{-2}$

A. Twisted String Actuator

Given the unwound length l_u and the cross-section radius of the string r_s, the actuator length is given by

$$l_s(\theta_s) = \sqrt{l_u^2 - \theta_s^2 r_s^2} \tag{1}$$

where θ_s is the motor angle, as shown in figure 1. This equation assumes an infinite string stiffness, so is only reasonably accurate under low tension. Although theoretically the stroke of the TSA can be the entire domain of $[0, l_u]$, in reality the thickness of the string prevents a geometric helix from forming once the helix pitch $q < 4r_s$ (or $q < 2nr_s$ for n strings) as mentioned in [4]. This limits the lower bound of the stroke as follows,

$$l_{\min} = \frac{l_u}{\sqrt{\frac{\pi^2}{2} + 1}} \approx 0.46\ l_u \tag{2}$$
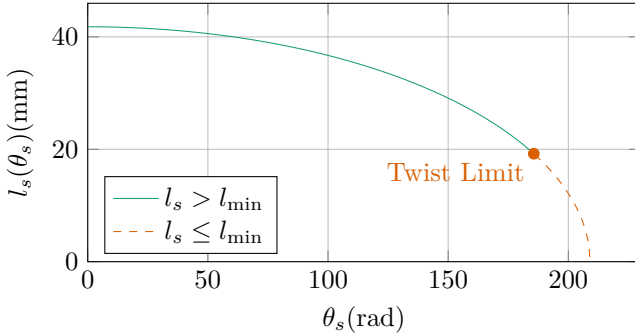
or approximately 46% of l_u for a two string TSA.

Fig. 1: TSA string length against motor angle with coefficients from table I.

B. Antagonistic Triad

As mentioned in the introduction, because the TSA provides only tensile force, a minimum of three actuators are required for a 2 DOF actuation system. These can be arranged in a triangular configuration to create an "antagonistic triad", akin to the antagonistic pairs of muscles found in animals. In a pair arrangement, one actuator contracts while the other relaxes, but in a triad, up to two actuators can share the same action, and one actuator can be inactive if the other two are performing different actions. The geometric structure of the system as shown in figure 2 can be described with two equilateral triangles of inradius r on two planes separated in the z axis. The centroids are then connected via a universal joint from each plane normal to an intersecting point, let the vector $\boldsymbol{\theta} = \begin{bmatrix} \theta_1 & \theta_2 \end{bmatrix}$ denote the rotation of the second plane relative to the first, in the y and x axes around the intersecting point, and let l_1 and l_2 denote the normal distance from the intersection to the first and second plane centroids respectively. When $\boldsymbol{\theta} = \begin{bmatrix} 0 & 0 \end{bmatrix}$ the triangles are parallel to each other. The distance between the vertex pairs of each triangle is then denoted as $\begin{bmatrix} \lambda_1 & \lambda_2 & \lambda_3 \end{bmatrix}$ for the "top", "left" and "right" vertices of the triangles. When $\boldsymbol{\theta}$ is changed, this will change λ_1, λ_2 and λ_3 respectively.

To calculate the lengths of the strings for a given $\boldsymbol{\theta}$ of the universal joint, we define a vector function $\Lambda(\boldsymbol{\theta}) = \begin{bmatrix} \lambda_1(\boldsymbol{\theta}) & \lambda_2(\boldsymbol{\theta}) & \lambda_3(\boldsymbol{\theta}) \end{bmatrix}$ as follows.

$$\lambda_1(\boldsymbol{\theta}) = \sqrt{\begin{array}{l} (l_1 + l_2 \cos\theta_1 \cos\theta_2 + r\cos\theta_1 \sin\theta_2)^2 \\ + (r - r\cos\theta_2 + l_2 \sin\theta_2)^2 \\ + (l_2 \cos\theta_2 \sin\theta_1 + r\sin\theta_1 \sin\theta_2)^2 \end{array}}$$

$$\lambda_2(\boldsymbol{\theta}) = \sqrt{(a - b + c)^2 + (l_1 - d)^2 + e^2}$$

$$\lambda_3(\boldsymbol{\theta}) = \sqrt{(a + b - c)^2 + (l_1 + d)^2 + e^2} \tag{3}$$

where:

$$a = -\frac{\sqrt{3}r(\cos\theta_1 - 1)}{2}$$
$$b = l_2 \cos\theta_2 \sin\theta_1$$
$$c = \frac{r\sin\theta_1 \sin\theta_2}{2}$$
$$d = \frac{\sqrt{3}r\sin\theta_1}{2} + l_2 \cos\theta_1 \cos\theta_2 - \frac{r\cos\theta_1 \sin\theta_2}{2}$$
$$e = \frac{r\cos\theta_2}{2} - \frac{r}{2} + l_2 \sin\theta_2$$

Surface plots of the functions in (3) are shown in figure 3 for a domain of $\left[-\frac{\pi}{2}, \frac{\pi}{2}\right]$.

II. CONTROL SYSTEM

The control system is a four layer cascade design, joining an inverse dynamic control system [9], to the triad force controller in [10], to a proprtional controller for each TSA. It uses feedback signals of the joint position from the accelerometers and TSA force from the load cells. A second order setpoint trajectory $\boldsymbol{q}$ is used as the input, which can either be pre-defined or generated dynamically from user input. Feedback is provided by the AUJ angular position $\boldsymbol{\theta}$ as shown in figure 2, angular velocity $\dot{\boldsymbol{\theta}}$, and TSA tension force $\hat{\boldsymbol{f}}$. Figure 4 shows a complete block diagram of the control system.

A. Actuated Universal Joint Position PID Controller with Acceleration Feedforward

Firstly, a PID controller is used to generate a control signal $\boldsymbol{u}$ with the input $\boldsymbol{q}$ as the setpoint, and the AUJ
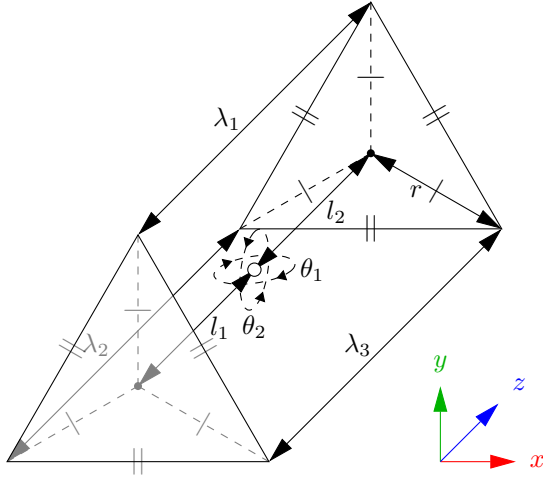
Fig. 2: Kinematic diagram of the antagonistic triad, where the universal joint rotation is defined by $\theta_{1,2}$ on the y and x axes respectively, and the actuator lengths are defined by $\lambda_{1,2,3}$ for the "top", "left" and "right" actuators. r and $l_{1,2}$ define the anchor points of the actuators.

angular position $\boldsymbol{\theta}$ and velocity $\dot{\boldsymbol{\theta}}$ as feedback, plus the addition of a feedforward term for the input acceleration $\ddot{\boldsymbol{q}}$, i.e.

$$u = k_p \left(\boldsymbol{q} - \boldsymbol{\theta}\right) + k_i \left(\int_0^t \left(\boldsymbol{q} - \boldsymbol{\theta}\right) dt\right) + k_d \left(\dot{\boldsymbol{q}} - \dot{\boldsymbol{\theta}}\right) + \ddot{\boldsymbol{q}}. \tag{4}$$

B. Inverse Dynamics

The control signal $\boldsymbol{u}$ from the PID controller is then converted to the desired AUJ torque $\boldsymbol{\tau}$ as follows

$$\boldsymbol{\tau} = D\left(\boldsymbol{\theta}\right) \boldsymbol{u} + C\left(\boldsymbol{\theta}, \dot{\boldsymbol{\theta}}\right) \dot{\boldsymbol{\theta}} + G\left(\boldsymbol{\theta}\right). \tag{5}$$

C. Twisted String Actuator Force Optimisation Algorithm

This uses a modified algorithm from [10], which proposes an inverse force transformation algorithm to control an antagonistic triad using force controlled linear actuators, to select an optimal force vector from the desired joint torque. A force matrix $\boldsymbol{F}$ is created from the torque input $\boldsymbol{\tau}$, jacobian J_Λ from the vector function Λ as defined in (3), and minimum force constant $f_{\min}$. The diagonal components $f_{i,i}$ are equal to $f_{\min}$, while the other elements in the column are based on a calculation using $J_{\Lambda-i,*}$ where $-i$ is a row removed from the matrix.

$$J_\Lambda = \begin{bmatrix} \frac{\partial \lambda_1}{\partial \theta_1} & \frac{\partial \lambda_2}{\partial \theta_1} & \frac{\partial \lambda_3}{\partial \theta_1} \\ \frac{\partial \lambda_1}{\partial \theta_2} & \frac{\partial \lambda_2}{\partial \theta_2} & \frac{\partial \lambda_3}{\partial \theta_2} \end{bmatrix}$$

$$\boldsymbol{\gamma}\left(i\right) = -J_{\Lambda-i,*}^{-\mathsf{T}} \left(J_{\Lambda i,*}^{\mathsf{T}} f_{\min} + \boldsymbol{\tau}\right) \tag{6}$$

$$\boldsymbol{F}\left(\boldsymbol{\tau}, \boldsymbol{\theta}\right) = \begin{bmatrix} f_{\min} & \boldsymbol{\gamma}\left(2\right)_1 & \boldsymbol{\gamma}\left(3\right)_1 \\ \boldsymbol{\gamma}\left(1\right)_1 & f_{\min} & \boldsymbol{\gamma}\left(3\right)_2 \\ \boldsymbol{\gamma}\left(1\right)_2 & \boldsymbol{\gamma}\left(2\right)_2 & f_{\min} \end{bmatrix}$$

The following algorithm then selects one column of $\boldsymbol{F}$ to be the output force vector $\boldsymbol{f}$, where $\top$ and $\perp$ are boolean *true* and *false* respectively

1: $\boldsymbol{s} \leftarrow \begin{bmatrix} \top & \top & \top \end{bmatrix}$
2: **if** $f_{23} > f_{\min}$ **then** $s_2 \leftarrow \perp$ **else** $s_3 \leftarrow \perp$ **end if**
3: **if** $f_{31} > f_{\min}$ **then** $s_3 \leftarrow \perp$ **else** $s_1 \leftarrow \perp$ **end if**
4: **if** $f_{12} \geq f_{\min}$ **then** $s_1 \leftarrow \perp$ **else** $s_2 \leftarrow \perp$ **end if**
5: **for** $i = 1$ to 3 **do**
6:      **if** $s_i \rightarrow \top$ **then** $\boldsymbol{f} \leftarrow \boldsymbol{f}_{*,i}$ **end if**
7: **end for**

D. Twisted String Actuator Force Proportional Controller

The selected forces are then used as an input to a P controller with gain k_{p_s} using the measured load cell forces $\hat{\boldsymbol{f}}$ as feedback. The output from this can then be used to control the top, left and right TSA motors, corresponding to the actuators in figure 2.

1) Simulation Current Control: In the simulation, each TSA was modelled as a state-space system which takes motor current u as an input and outputs y as the TSA tension force. [4] defines it as such, where J is the motor inertia, C is the motor coulomb friction (modified from viscous friction as the motor only has dry friction), K_t is the motor torque constant, and K_L is the load stiffness. As the original definition is for a fixed load l_u distance from the motor a modified model is required which takes into account the varying length between the motor and load defined by $\Lambda\left(\boldsymbol{\theta}\right)$. A saturation function, with the compact notation $\text{sat}_x^y z = \max\left(x, \min\left(y, z\right)\right)$ is used to prevent incorrect compression forces when the string is slack. All of the motor coefficients were taken from the Faulhaber 1724TSR datasheet [11] as this is the motor used in the experimental model. An estimated value is used for the load stiffness, this was chosen to be a high number as the model is expected to be very stiff.

$$h\left(\theta_s\right) = \frac{\theta r_s^2}{\sqrt{l_u^2 - \theta_s^2 r_s^2}}$$

$$k\left(\theta_s, \boldsymbol{\theta}\right) = \lambda_n\left(\boldsymbol{\theta}\right) - \sqrt{l_u^2 - \theta_s^2 r_s^2}$$

$$\dot{\boldsymbol{x}} = \begin{bmatrix} x_2 \\ -\frac{K_L}{J} h\left(x_1\right) k\left(x_1, \boldsymbol{\theta}\right) - \frac{C}{J} \operatorname{sgn}\left(x_2\right) \end{bmatrix} + \begin{bmatrix} 0 \\ \frac{K_t}{J} \end{bmatrix} u$$

$$y = K_L \operatorname{sat}_0^\infty k\left(x_1, \boldsymbol{\theta}\right) \tag{7}$$

The state space model was then adapted to include constraints on motor velocity and acceleration set by the motor controller in order to keep the motor within design limits, by replacing $\dot{\boldsymbol{x}}$ with $\dot{\boldsymbol{x}}'$ which contains saturation functions for maximum motor velocity v_s and acceleration α_s.

$$\dot{\boldsymbol{x}}' = \begin{bmatrix} \operatorname{sat}_{-\omega_s}^{\omega_s} \dot{x}_1 \\ \operatorname{sat}_{-\alpha_s}^{\alpha_s} \dot{x}_2 \end{bmatrix} \tag{8}$$

2) Experimental Velocity Control with Deadband Compensation: Due to a controller deadband within $\pm 10\,\text{min}^{-1}$, an adjustable deadband compensator is used,
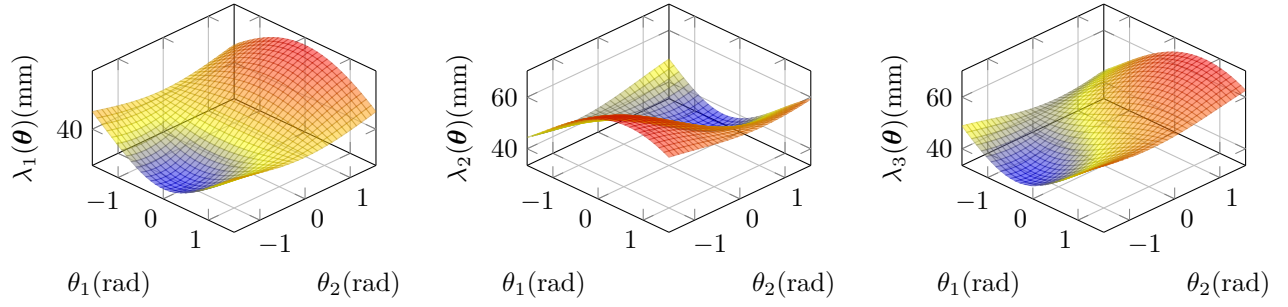
Fig. 3: Surface plots of each element of the vector function $\Lambda(\boldsymbol{\theta})$, assuming coefficient values from table I. Note that λ_2 and λ_3 are symmetric.
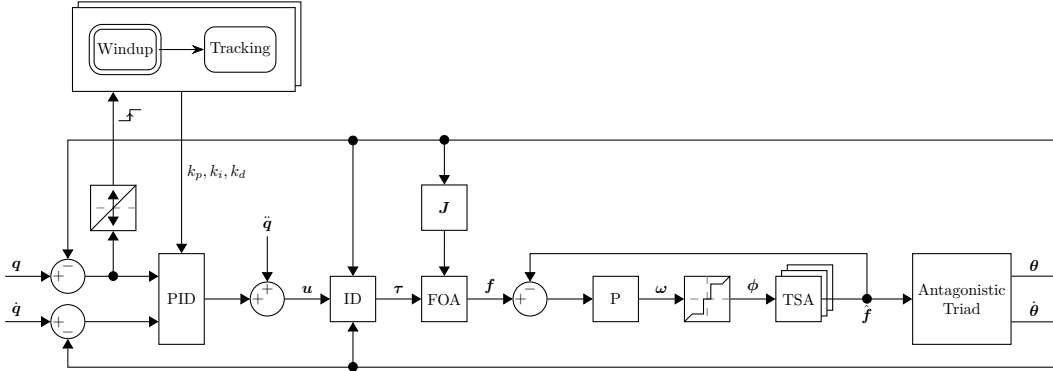

Fig. 4: Block diagram of the complete experimental control system, excluding the hardware velocity controllers for the motors.

TABLE II: PID gains in the simulation and experiment.

Gain	Value	
	Simulation	Experiment*
k_p	800	3×10^4
k_i	3000	350
k_d	50	50
k_{p_s}	19	100

* Tracking mode, see section III-B.

$$\phi_i(\omega_i) = \begin{cases} 10 & 10 \leq \omega_i < h \\ -10 & -h < \omega_i \leq -10 \\ 0 & h \leq \omega_i \leq -h \\ \omega_i & \text{otherwise} \end{cases} \tag{9}$$

where ϕ_i is the compensator for the controller i. An adjustment value $h \in [0, 10]$ changes the threshold at which the compensator switches on and off, allowing for a small deadband to remain.

The result from the TSA is then a compressive force acting between each of the three TSA and its corresponding endpoint on the Antagonistic Triad, imparting a torque on the axes of the universal joint.

III. Simulation & Experimental Results

A. Experimental Setup

For the experimental validation, a physical prototype of the mechanism was constructed with coefficients from table I as design parameters. This was mounted vertically, in order for the Inertial Measurement Unit (IMU) to measure the orientation of the universal joint. The TSA mechanisms consist of a compact high torque motor attached to the base segment, with a string clamp attached to the motor shaft. On the follower segment, a load cell is mounted on top of a universal joint to ensure a purely axial load, with a capstan bolt attached to the load cell. The string itself is attached to the clamp at both ends using two grub screws for extra security and easy adjustment, and looped through the hole in the capstan bolt. The total mass of the prototype, excluding the mount, is ≈ 176 g. Figure 8 details the construction of the experiment with all the constituent parts.

B. Windup & Tracking States

The tracking controller is activated after a "wind up" stage when the operating conditions are met. The controller parameters for the Windup and Tracking states are $k_p = 800$, $k_i = 3000$, and $k_p = 3 \times 10^4$, $k_i = 350$ respectively. This transition trigger is defined on a per-axis basis, as the first zero crossing of the angle error

(as $\boldsymbol{q} = 0$ this is effectively $\boldsymbol{\theta}$). A graph showing the difference this state change makes to the AUJ orientation is shown in figure 5.
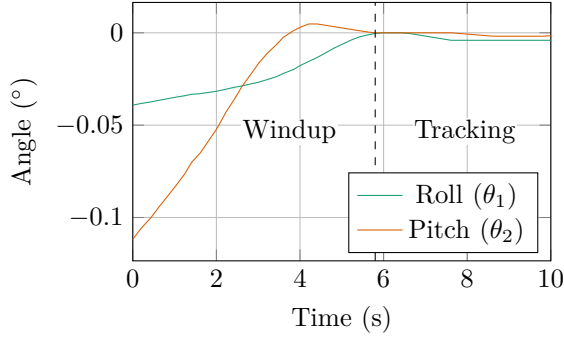

Fig. 5: The inital startup of the mechanism showing the transition between "windup" and "tracking" states.

C. Results

Figure 6 plots the tracking response of both the simulation and experiment. Three trajectories were created to test the capabilities of the mechanism. Two were only in one axis of the Universal Joint, and the third was in both axes. The deflection angle range was limited to $\pm11°$ on a single axis, and $\pm6°$ on both axes. This was partly due to the low value of l_u, but can easily be extended by increasing this value, a low l_u was chosen as it resulted in easier installation.
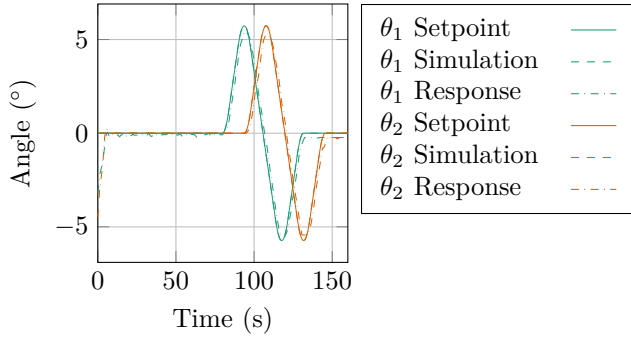

Fig. 6: Plot of the response for a roll θ_1 and pitch θ_2 trajectory. Note the simulation error is very small, so the plot cannot be seen on the graph.

IV. Performance Comparison

To compare the performance of a TSA AUJ against alternatives, we can measure two metrics, the maximum tension force $f_{\max}$ and maximum stroke velocity $\dot{p}_{\max}$. This corresponds to the equivalent of maximum torque and maximum velocity in a rotary motor, a larger $f_{\max}$ would be able to actuate a larger follower mass, and a larger $\dot{p}_{\max}$ would be able to rotate the AUJ more quickly. The alternatives chosen for comparison are leadscrews of various rod diameters d_m and pitches λ, and a "direct drive" where the motor is rotating the

universal joint directly without any reduction or motion transformation.

A. Twisted String Actuator

For the TSA metrics, the equations from [4], in particular $h(\theta)$ and $k(\theta)$ as used for the state space, which can be used to determine $f_{\max}$ and $\dot{p}_{\max}$. By extracting coefficient r_s as an input to make $f(p, r_s)$ and $\dot{p}(\dot{\theta}, p, r_s)$ the performance of different string thicknesses can be compared for a given unwound length l_u and $\tau_{\max}, \dot{\theta}_{\max}$ over the range of the contraction length p.

$$
\begin{aligned}
k^{-1}(p) &= \pm\frac{\sqrt{p(2l_u - p)}}{r_s} \\
h^{-1}(\theta) &= \frac{\sqrt{l_u^2 - r_s^2\theta^2}}{r_s^2\theta} \\
f(p) = h^{-1}\left(k^{-1}(p)\right) &= \pm\frac{\sqrt{(l_u - p)^2}}{r_s\sqrt{p(2l_u - p)}} \\
f_{\max} &= f(p)\tau_{\max}
\end{aligned} \tag{10}
$$

$$
\begin{aligned}
\dot{k}\left(\dot{\theta}, \theta\right) &= \frac{\dot{\theta}r_s^2\theta}{\sqrt{l_u^2 - r_s^2\theta^2}} \\
\dot{p}\left(\dot{\theta}, p\right) = \dot{k}\left(\dot{\theta}, k^{-1}(p)\right) &= \pm\frac{\dot{\theta}r_s\sqrt{p(2l_u - p)}}{\sqrt{(l_u - p)^2}} \\
\dot{p}_{\max} &= \dot{p}\left(\dot{\theta}_{\max}, p\right)
\end{aligned} \tag{11}
$$

B. Leadscrew

For the leadscrew metrics, the raising torque calculation [12] can be used as the absolute value of $f_{\max}$, since the TSA only operates in tension, which can be used to determine the same metrics. The performance of different screw diameters d_m and leads λ can then be compared for a given $\tau_{\max}$ and coefficient of friction μ. $\dot{p}_{\max}$ is then calculated by multiplying λ with $\dot{\theta}_{\max}$. The performance of different λ can then be compared for a given $\dot{\theta}_{\max}$.

$$
\begin{aligned}
|\tau(f)| &= \frac{d_m f(\lambda + \pi d_m\mu)}{2(\pi d_m - \lambda\mu)} \\
|f(\tau)| &= \frac{2\tau(\pi d_m - \lambda\mu)}{d_m(\lambda + \pi d_m\mu)} \\
f_{\max} &= |f(\tau_{\max})|
\end{aligned} \tag{12}
$$

$$
\begin{aligned}
\dot{p}\left(\dot{\theta}\right) &= \lambda\frac{\dot{\theta}}{2\pi} \\
\dot{p}_{\max} &= \dot{p}\left(\dot{\theta}_{\max}\right)
\end{aligned} \tag{13}
$$

C. Direct Drive

The direct drive metrics are trivially calculated using the lever force and tangential velocity that would be generated at the endpoint of a linear actuator able to impart equivalent angular velocity and torque on the universal joint.
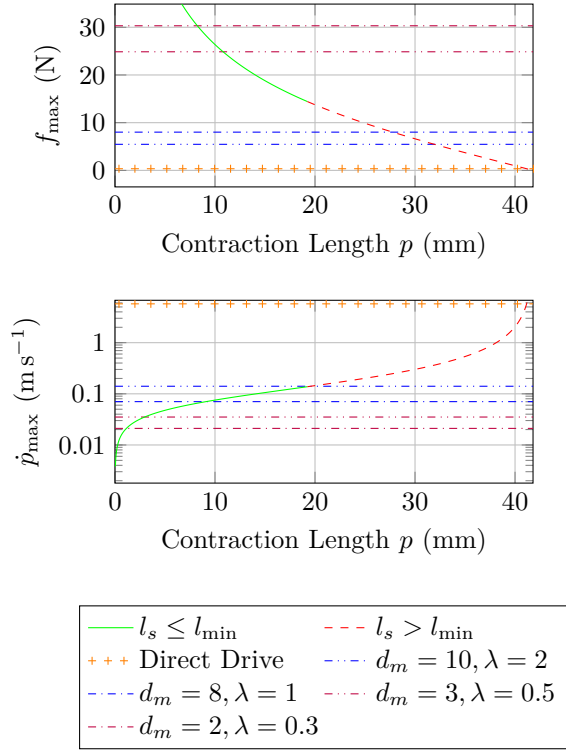
Fig. 7: Performance comparison of the TSA configuration using coefficients from table I to various leadscrew configurations with different d_m and λ, and the direct drive, where $\mu = 0.1$ for the leadscrews.

$$f_{\max} = \frac{\tau_{\max}}{\sqrt{l_2^2 + r^2}} \tag{14}$$

$$\dot{p}_{\max} = \dot{\theta}_{\max}\sqrt{l_2^2 + r^2} \tag{15}$$

D. Comparison

As the values for $\tau_{\max}$ and $\dot{\theta}_{\max}$ for the TSA depend on p, but remain constant for the leadscrew, the performance of the TSA is going to be better or worse than a given leadscrew depending on the value p. Figure 7 compares the TSA configuration using the coefficients from table I against a number of common leadscrew configurations that are practical for the dimensions of the AUJ. The TSA outperforms or underperforms different leadscrew configurations depending on p. In simpler terms, the performance of the TSA is dependent on the contraction length. The maximum linear velocity increases with the contraction length, and the maximum tension force decreases with contraction length, both in an nonlinear fashion.

V. CONCLUSION

This research has demonstrated the robust control of the orientation of a universal joint using TSA in an antagonistic triad configuration, with a low tracking error ($\pm 1.8°$) at low speed (max. $0.6°\,\mathrm{s}^{-1}$) in 2 DOF control with a vertical base orientation. It has also compared the
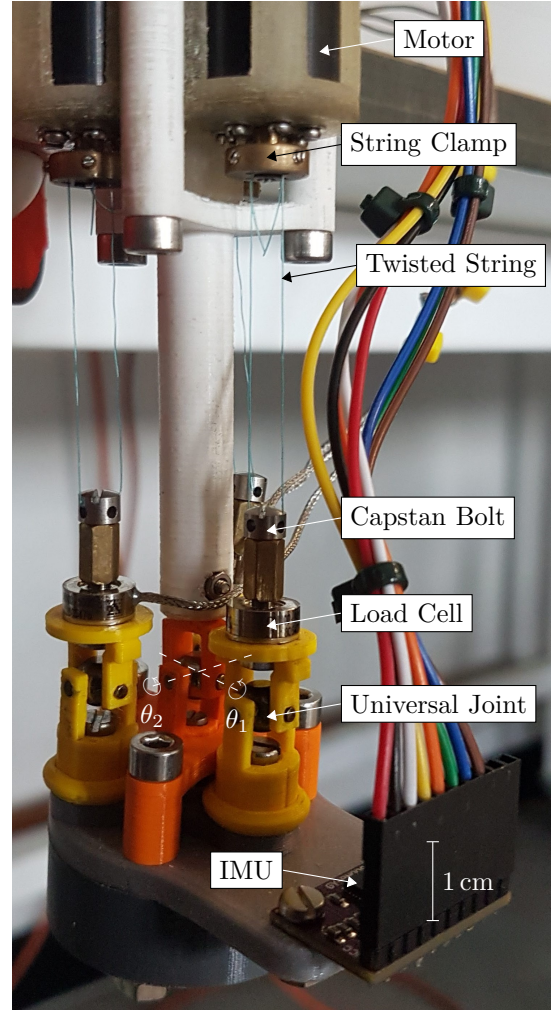

Fig. 8: Annotated photograph of the experimental model, with the roll θ_1 and pitch θ_2 axes marked.

performance of the system to alternative actuation methods. Future developments would include improvements to the orientation sensors, the data from the IMU proved to be unreliable and of poor resolution, so either a superior IMU will be used or an alternative method for sensing the universal joint orientation will be investigated, such as Linear Variable Differential Transformers (LVDTs), hall effect sensors or potentiometers. The system was tested in a vertical base orientation in order for the IMU to be able to measure the joint orientation. With suitable modifications to the inverse dynamics function and a known base orientation, it will be possible to test the controller at non-vertical base orientations. We will also increase the joint velocity, joint range and follower mass (m) in order to test the performance of the system under more strenuous conditions. The controller performance will also be quantified, examining the open and closed loop bandwidth. Eventually, we wish to develop a system comprised of multiple segments, to demonstrate its suitability for applications such as mobile snake robots or continuum robots.

REFERENCES

[1] R. Buckingham and A. Graham, "Nuclear snake-arm robots," *Industrial Robot: An International Journal*, 2012.

[2] M. Luo, R. Yan, Z. Wan, *et al.*, "Orisnake: Design, fabrication, and experimental analysis of a 3-d origami snake robot," *IEEE Robotics and Automation Letters*, vol. 3, no. 3, pp. 1993–1999, 2018.

[3] W. S. Rone, W. Saab, and P. Ben-Tzvi, "Design, Modeling, and Integration of a Flexible Universal Spatial Robotic Tail," *Journal of Mechanisms and Robotics*, vol. 10, no. 4, Apr. 2018, 041001, ISSN: 1942-4302. DOI: 10.1115/1.4039500.

[4] T. Würtz, C. May, B. Holz, C. Natale, G. Palli, and C. Melchiorri, "The twisted string actuation system: Modeling and control," in *2010 IEEE/ASME International Conference on Advanced Intelligent Mechatronics*, 2010, pp. 1215–1220. DOI: 10.1109/AIM.2010.5695720.

[5] P. Muehlbauer, M. Schimbera, K. Stewart, and P. P. Pott, "Twisted string actuation for an active modular hand orthosis," in *ACTUATOR; International Conference and Exhibition on New Actuator Systems and Applications 2021*, VDE, 2021, pp. 1–4.

[6] J. Park, J.-i. Park, H.-T. Seo, Y. Liu, K.-S. Kim, and S. Kim, "Control of tendon-driven (twisted-string actuator) robotic joint with adaptive variable-radius pulley," in *2020 20th International Conference on Control, Automation and Systems (ICCAS)*, IEEE, 2020, pp. 1096–1098.

[7] B. Suthar and S. Jung, "Design and feasibility analysis of a foldable robot arm for drones using a twisted string actuator: Frad-tsa," *IEEE Robotics and Automation Letters*, vol. 6, no. 3, pp. 5769–5775, 2021. DOI: 10.1109/LRA.2021.3084890.

[8] S. Nedelchev, I. Gaponov, and J. Ryu, "Accurate dynamic modeling of twisted string actuators accounting for string compliance and friction," *IEEE Robotics and Automation Letters*, vol. 5, no. 2, pp. 3438–3443, 2020. DOI: 10.1109/LRA.2020.2970651.

[9] M. W. Spong, S. Hutchinson, and M. Vidyasagar, *Robot modeling and control*. John Wiley & Sons, 2020.

[10] F. Dessen, "Coordinating control of a two degrees of freedom universal joint structure driven by three servos," in *Proceedings. 1986 IEEE International Conference on Robotics and Automation*, vol. 3, 1986, pp. 817–822. DOI: 10.1109/ROBOT.1986.1087559.

[11] *Dc micromotors - precious metal commutation*, Dr. Fritz Fauhaber GmbH & Co. KG, Feb. 2020.

[12] J. Shigley, C. Mischke, and R. Budynas, *Mechanical Engineering Design* (McGraw-Hill series in mechanical engineering). McGraw-Hill, 2004, ISBN: 9780072520361.